

Quantum criticality of the Ising-like screw chain antiferromagnet $\text{SrCo}_2\text{V}_2\text{O}_8$ in a transverse magnetic field

Y. Cui,¹ H. Zou,² N. Xi,¹ Zhangzhen He,^{3,*} Y. X. Yang,⁴ L. Shu,^{4,5} G. H. Zhang,¹ Z. Hu,¹ T. Chen,¹ Rong Yu,¹ Jianda Wu,^{2,†} and Weiqiang Yu^{1,‡}

¹Department of Physics and Beijing Key Laboratory of Opto-electronic Functional Materials & Micro-nano Devices, Renmin University of China, Beijing, 100872, China

²Tsung-Dao Lee Institute & School of Physics and Astronomy, Shanghai Jiao Tong University, Shanghai, 200240, China

³State Key Laboratory of Structural Chemistry, Fujian Institute of Research on the Structure of Matter, Chinese Academy of Sciences, Fuzhou, Fujian 350002, China

⁴State Key Laboratory of Surface Physics, Department of Physics, Fudan University, Shanghai 200433, China

⁵Collaborative Innovation Center of Advanced Microstructures, Nanjing 210093, China

The quantum criticality of an Ising-like screw chain antiferromagnet $\text{SrCo}_2\text{V}_2\text{O}_8$, with a transverse magnetic field applied along the crystalline a -axis, is investigated by ultra-low temperature NMR measurements. The Néel temperature is rapidly and continuously suppressed by the field, giving rise to a quantum critical point (QCP) at $H_{C1} \approx 7.0$ T. Surprisingly, a second QCP at $H_{C2} \approx 7.7$ T featured with gapless excitations is resolved from both the double-peak structure of the field dependent spin-lattice relaxation rate $1/^{51}\text{T}_1$ at low temperatures and the weakly temperature-dependent $1/^{51}\text{T}_1$ at this field. Our data, combined with numerical calculations, suggest that the induced effective staggered transverse field significantly lowers the critical fields, and leads to an exposed QCP at H_{C2} , which belongs to the one-dimensional transverse-field Ising universality.

Novel quantum states with exotic excitations can emerge near a quantum phase transition [1–3]. As one prototype for quantum phase transitions and quantum criticality, the one-dimensional transverse-field Ising model (1DTFIM) has been widely investigated [4–12]. In this model, the magnetic order is suppressed by a transverse magnetic field, resulting in an order-disorder quantum phase transition, with gap closed at a quantum critical point (QCP), H_C . It has been predicted that a quantum E_8 integrable model emerges near the vicinity of the QCP when a weak longitudinal field is applied [13]. The experimental realization of such a QCP is yet challenging because the interchain exchange couplings in real materials usually stabilize the magnetic order at $T > 0$ and mask the genuine 1D quantum criticality. Nonetheless, a 1DTFIM-like QCP hidden in the 3D ordered phase was suggested in the ferromagnetic chain compound CoNb_2O_6 [14–16].

Recently, a class of Ising anisotropic antiferromagnetic screw chain compounds $\text{ACo}_2\text{V}_2\text{O}_8$ ($A = \text{Ba}, \text{Sr}$) [17, 18] attracts a lot of research attention. In these compounds, the easy-axis is along the chain direction (c -axis), and the intrachain exchange coupling $J_z \approx 5\text{--}7$ meV [19, 20]. Both compounds order at fairly low temperatures (about 5 K), which implies the interchain exchange coupling $J' \ll J$ [21–23]. The magnetic order can be suppressed by a transverse field applied in the ab -plane [17, 18]. Interestingly, the critical field values and the quantum critical behaviors are very different for fields applied along the [100] and the [110] direction [20, 24–30]. In $\text{BaCo}_2\text{V}_2\text{O}_8$, separated 3D and 1D QCPs were suggested with field along the [110] direction at $H \gtrsim 20$ T [29]. For the field along the [100] direction, $H_C \sim 10$ T [25], much lower

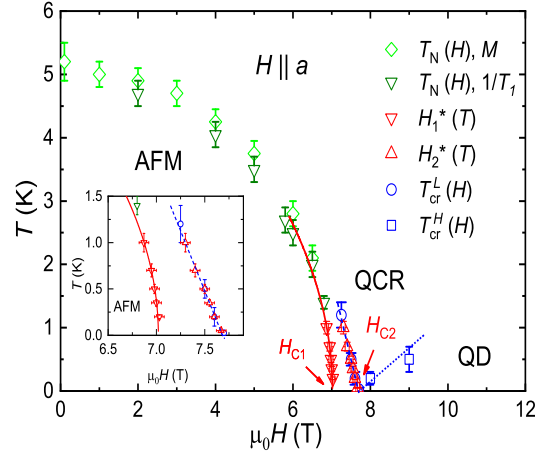


FIG. 1: Phase diagram of $\text{SrCo}_2\text{V}_2\text{O}_8$ in a transverse field along the a -axis. AFM, QCR and QD refer to the antiferromagnetic phase, the quantum critical regime, and the quantum disordered regime. Diamonds represent the Néel temperatures determined by the magnetization data. Down triangles, circles, and squares represent the Néel temperatures, the crossover temperatures T_{cr}^L and T_{cr}^H , respectively, all determined by the $1/^{51}\text{T}_1$ with different schemes of measurements (main text). The solid line is a function fit to $T_N \sim (H_{C1} - H)^{0.5}$ with $H_{C1} \approx 7.03$ T. The blue lines denote function fits to $T_{cr}^{L,H} \sim |H_{C2} - H|$ with $H_{C2} \approx 7.7$ T. Inset: An enlarged view of the fitting.

than the H_C along the [110] direction. With field along the [100] direction, the linear confining potential arising from the interchain correlation at fields below H_C , and the paramagnetism at fields above H_C , create different topological excitations [27, 31]. The critical behavior near H_C is, however, not investigated.

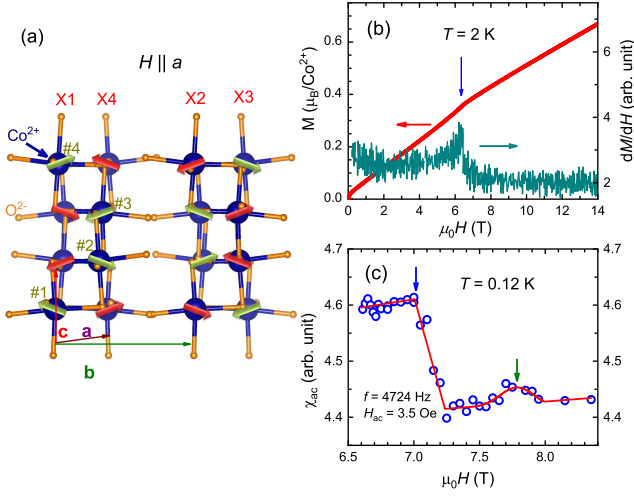


FIG. 2: (a) A schematic drawing of a unit cell of SrCo₂V₂O₈. *a*, *b* and *c* label the tetragonal axes, X1 to X4 label four neighboring spin chains. #1 to #4 label the Co²⁺ sites along one screw chain. The arrows placed on the Co²⁺ sites mark the direction of the effective staggered field created by a *dc* field applied along the *a*-axis. (b) The *dc* magnetization *M* vs. *H* at 2 K and its derivative with the field. The arrow marks a peaked feature in *dM/dH*. (c) The *ac* susceptibility χ_{ac} as a function of *H* at 0.12 K. The arrows mark a sharp drop and a round peak in the data, respectively.

In order to reveal the properties in the critical regime, low-temperature and low-energy probes are desired. Here we report our susceptibility and ⁵¹V NMR measurements on SrCo₂V₂O₈ with *H* || *a* and temperatures down to 50 mK. The main results are summarized in the phase diagram of Fig. 1. From the double-peak signature of the $1/^{51}T_1$ data, we identify two QCPs at $H_{C1} \approx 7$ T and $H_{C2} \approx 7.7$ T, respectively. By analyzing the NMR line splitting at low temperatures, we show that the system establishes three dimensional (3D) magnetic ordering below H_{C1} and the paramagnetic phase above H_{C2} . In between H_{C1} and H_{C2} , the line splitting is absent. We observe $1/^{51}T_1 \sim T^{2.2}$ at H_{C1} and becomes almost temperature-independent at H_{C2} , signaling gapless excitations at these two QCPs. Our experiment reveals highly nontrivial critical behaviors of the system, and hence discovers a new route in accessing novel quantum criticality in quasi-1D Ising-like antiferromagnets, accomplished from screwed lattice structures.

The *dc* magnetization was measured above 2 K and the *ac* susceptibility was measured at 0.12 K. Detailed NMR sample preparation and measurement techniques are described in Sec. S1 [32]. The ⁵¹V ($I = 7/2$, $^{51}\gamma = 11.198$ MHz/T) NMR were performed in a dilution refrigerator with the spin-echo technique. The spin-lattice relaxation rate $1/^{51}T_1$ were measured by the inversion-recovery method, where the nuclear-magnetization is well fit with the recovery function for $I = 7/2$ spins [33, 34] without any stretching behavior, indicating high-quality

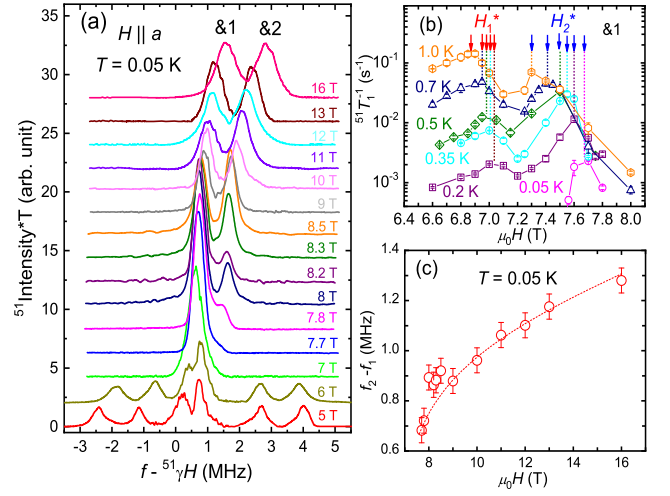


FIG. 3: (a) The ⁵¹V NMR spectra measured at 0.05 K with typical fields. Escalated vertical offsets are applied for clarity. &1 and &2 mark the two resonance peaks at fields above 7.7 T. (b) The field-dependence of $1/^{51}T_1$ at fixed temperatures measured on peak &1. H_1^* and H_2^* mark the field locations of peaked $1/^{51}T_1$ at each temperature. (c) The frequency difference between peak &1 and &2 as a function of field.

of the sample (Sec. S8 [32]).

SrCo₂V₂O₈ crystallizes in a tetragonal space group *I*4₁*cd* [18] as shown in Fig. 2(a). It consists of screwed chains along the *c*-axis with alternative clockwise and anticlockwise screwing directions among neighboring chains [21]. Each unit cell contains four chain segments in the *ab*-plane (labeled as X1 to X4), and each of them further includes four sites labeled as #1 to #4. Similar to SrCo₂V₂O₈, the primary interactions can be formulated as a 3D spin-1/2 antiferromagnetic XXX model with strong Ising anisotropy (along the *c*-axis) (Sec. S2 [32]). Because the vertical O-Co-O bond of SrCo₂V₂O₈ in the local CoO₆ octahedral tilts from the *c*-axis by $\sim 5.1^\circ$ with a four-site period [35], the applied *a*-axis transverse field *H* induces a staggered field H_y along the *b*-axis and a four-period field H_z along the *c*-axis [24], as demonstrated in Fig. 2(a).

The applied and induced staggered fields suppress the antiferromagnetic Ising order [24], leading to a phase transition, signaled in our magnetization data. The Néel temperatures determined from the magnetization data at different fields (Sec. S3 [32]) are plotted in Fig. 1. At 2 K, the *dc* magnetization is shown as a function of field in Fig. 2(b), which exhibits a kinked feature at about 6.4 T. The *dM/dH* clearly resolves a peak at 6.4 T, consistent with a field-induced phase transition as reported earlier [18, 21]. The *ac* susceptibility data at 0.12 K, as shown in Fig. 2(c), demonstrate a sharp drop at $\mu_0 H \approx 7$ T, indicating a quantum phase transition. In addition, we also observe a weak round peak at $\mu_0 H \approx 7.7$ T, indicating a crossover rather than a phase tran-

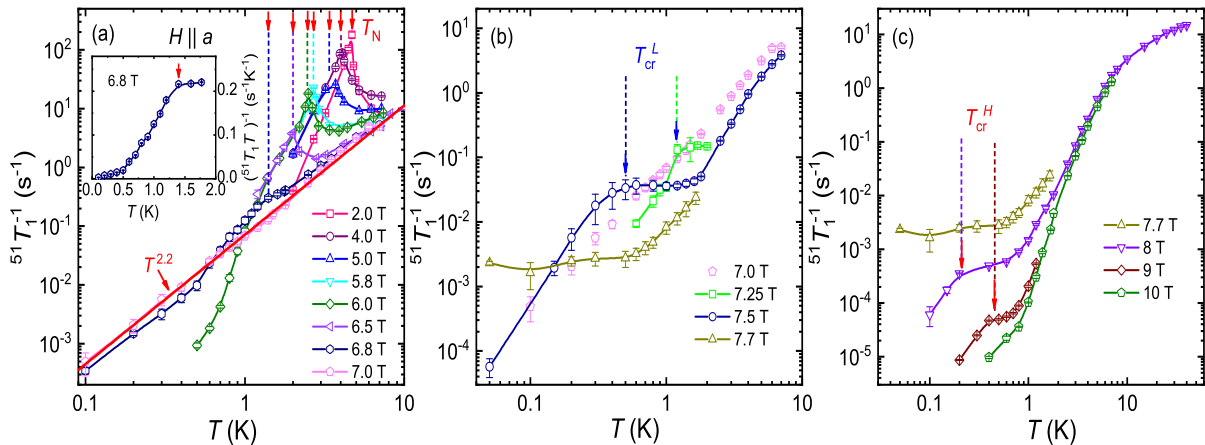


FIG. 4: The spin-lattice relaxation rate $1/^{51}T_1$ as functions of temperatures at various fields. (a) Data at fields below 7 T. The red arrows mark the peaked feature at T_N . The red straight line is a power-law function fit to the data at 7 T with $1/T_1 \sim T^\alpha$ ($\alpha=2.2$). Inset: T_N at 6.8 T resolved by a sharp drop of $1/^{51}T_1 T$ upon cooling. (b) Data at fields from 7 T to 7.7 T. (c) Data at fields above 7.7 T. T_{cr}^L (T_{cr}^H) at each field marks a crossover temperature between a gapped to a gapless behavior.

sition, which is a precursor to a 1D QCP and will be discussed in more details later. In the following, we show unambiguous evidence for distinctive magnetic behaviors separated by 7 T and 7.7 T by the ^{51}V NMR spectra and the spin-lattice relaxation rate $1/^{51}T_1$.

The ground state at each field can be distinguished by the NMR spectra at low temperatures. The ^{51}V spectra at frequencies close to $^{51}\gamma H$ are measured at typical fields and shown in Fig. 3(a). Three regimes are clearly seen. (1) Below 7 T, the ^{51}V spectra have six peaks. Such a line splitting is caused twinned magnetic domains in the ordered phase originating from frustrated interchain exchange couplings [32, 36]; (2) In the intermediate field range from 7 to 7.7 T, a single NMR line is seen close to the central frequency $f \approx ^{51}\gamma H$, which suggests the absence of magnetic ordering; (3) At fields above 7.7 T, two NMR lines, labeled as &1 and &2 in Fig. 3(a), emerge with increasing fields, and is also seen at temperature above 10 K (Fig. S8 [32]). The frequency difference of two peaks are depicted as a function of field in Fig. 3(c), which rises with field above 7.7 T, consistent with the paramagnetic phase (Sec. S7 [32]).

The magnetic transition at each field can be resolved by $1/^{51}T_1$, which is measured at the primary peak of the spectra. In Fig. 4(a)-(c), the $1/^{51}T_1$ with increasing temperature is shown at various fields. For fields below 6.5 T, a peak is observed in $1/^{51}T_1$, which determines the magnetic ordering temperature T_N . At 6.8 T, although a sharp drop of $1/T_1$ is not clearly discernible, the magnetic transition is resolved by a sudden drop of $1/^{51}T_1 T$ at 1.35 K, as demonstrated in the inset of Fig. 4(a). For any fields above 7 T, no peaked feature in the $1/^{51}T_1$ is observed, indicating the absence of magnetic ordering. The determined T_N with the fields up to 6.8 T is shown in Fig. 1. It agrees well with T_N determined from our dc

susceptibility data (Sec. S3 [32]).

To determine the transition precisely, we perform a field scan of $1/^{51}T_1$ at fixed T with increasing field and the result is shown in Fig. 3(b). Surprisingly, at low temperatures the $1/^{51}T_1$ curve shows two prominent peaks with field. For instance, at 0.2 K, a low-field peak is at ~ 7 T (marked as H_1^*), while a high-field one is at ~ 7.6 T (marked as H_2^*). These are close to the critical and the crossover field in the susceptibility data, respectively (see Fig. 2(c)). We then plot $H_1^*(T)$ and $H_2^*(T)$ as functions of temperatures in the phase diagram of Fig. 1.

The $H_1^*(T)$ line, together with the high-temperature T_N data, portray the critical trajectory, which is well fit by $T_N \sim (H - H_{C1})^\phi$ with $H_{C1} = 7.03$ T and a critical exponent $\phi \approx 0.5 \pm 0.09$. Taking into account that the absence of the NMR line splitting, the peaked feature in the $1/^{51}T_1(H)$, the sharp drop of χ_{ac} , and the mean-field-like exponent $\phi \approx 0.5$, all emerge at the same field $H_{C1} \approx 7$ T, we conclude that H_{C1} is a (3+1)D Ising critical point.

The determined T - H curve from $H_2^*(T)$ follows a straight line, as shown in Fig. 1. Given that no singularity of any thermodynamic quantities were observed, we understand it as a crossover approaching to a 1D QCP at $H_{C2} \approx 7.7$ T. This H_{C2} is also consistently resolved by the temperature evolution of $1/^{51}T$ data at different fields, as shown in Fig. 4. For fields either below or above H_{C2} , upon warming, the $1/^{51}T_1$ increases rapidly, and then crossovers to a weakly temperature-dependent behavior. This clearly indicates a gapped behavior below the crossover temperature T_{cr}^L (for $H < H_{C2}$) or T_{cr}^H (for $H > H_{C2}$) in Fig. 4(b), and in Fig. 1. T_{cr}^L decreases with field, while T_{cr}^H increases with field. Interestingly, T_{cr}^L overlaps with the crossover line $H_2^*(T)$ in the studied temperature regime. It scales linearly with field by

$T_{cr}^L \sim |H - H_{C2}|$, implying the critical exponents $\nu z = 1$, consistent with the 1DTFIM universality class [2].

In the following, we show how the transitions at these two QCPs are affected by the induced staggered fields. First, the existence of a 1D QCP at a low field is further supported by our theoretical calculation. We model the primary interactions of $\text{SrCo}_2\text{V}_2\text{O}_8$ to a spin-1/2 Heisenberg-Ising chain, and the effective Hamiltonian reads as,

$$H = \sum_i J[S_i^x S_{i+1}^x + S_i^y S_{i+1}^y + \Delta S_i^z S_{i+1}^z] - \mu_B g_x \sum_i [H S_i^x + H_y (-1)^i S_i^y + H_z S_i^z \cos(\pi(2i-1)/4)] \quad (1)$$

with $J \approx 3.7$ meV and the anisotropic factor $\Delta \approx 2.1$ [21, 24, 28, 37]. Here g_x is the gyromagnetic ratio, H is the applied field along the a -axis, H_y and H_z are, respectively, induced two- and four-period staggered fields along the b - and c -axis, due to screwed lattice structures [24]. By fitting the high-field magnetization data [39], we deduced $g_x \approx 3.7$, $H_y \approx 0.29 H$, and $H_z \approx 0.14 H$. We then apply the infinite time evolving block decimation (iTEBD) method [38] to determine the local static moment with respect to the field at zero temperature, shown in Sec. S4 [32]. The long-range antiferromagnetic order is continuously suppressed to zero at $H_C \approx 7.6$ T. Note that the calculated H_C value is very close to the measured H_{C2} . Compared to $H_C \sim 40$ T for $H \parallel [110]$, the H_C for $H \parallel [100]$ is largely reduced, and this is primarily caused by the induced staggered field H_y , which is the strongest for $H \parallel [100]$ and tuned down to zero for $H \parallel [110]$ [24].

Secondly, the scaling of the order parameter at H_C from the iTEBD calculation finds the critical exponent $\beta \approx 1/8$ (Fig. S6 [32]). This indicates that though H_C can be substantially reduced by the staggered field H_y , the QCP is still governed by the 1DTFIM universality [31, 32]. This is consistent with the linear scaling relation between the crossover temperature and the field found in experiment.

Lastly, in quasi-1D systems, the locations of 1D and 3D QCPs reflect the competition between the effective interchain couplings and the external and induced fields, and are usually strongly material dependent. For example, the 1D QCP of CoNb_2O_6 is hidden inside a magnetically ordered phase close to a 3D QCP [14]. In $\text{BaCo}_2\text{V}_2\text{O}_8$ with a transverse field applied along the [110] direction, a 3D QCP is located at about 20 T, succeeded by a 1D QCP at about 40 T [29]. For $\text{SrCo}_2\text{V}_2\text{O}_8$, given its similar structural and magnetic properties to $\text{BaCo}_2\text{V}_2\text{O}_8$, two QCPs with field along the [110] direction are expected although not explored. By rotating the field from the [110] to the [100] direction, the induced staggered field may significantly lower both QCPs, and our measurements unambiguously show that the 1D QCP is out-

side the 3D ordered phase, yet are separated by a small field of 0.7 T.

The observation of the 1D QCP outside the 3D ordered phase prompts that the effective interchain couplings are very weak. This is likely caused by the heavy frustration among the interchain couplings [21, 28]. The induced staggered fields, which are tied up with the screwed structure, may further enhance the frustration effects and help weaken the 3D order. However, a full discussion on this would need detailed information on the interchain couplings, which is beyond the scope of this paper.

In what follows, we discuss the spin dynamics at both the 1D and 3D QCPs. As for the 3D QCP at H_{C1} , our $1/^{51}\text{T}_1$ data exhibit a power-law scaling $1/^{51}\text{T}_1 \sim T^{2.2}$ from 10 K down to 0.1 K (Fig. 4(a)). Such a power-law scaling over two decades of temperatures also strongly evidences gapless excitations at H_{C1} . At the 1D QCP, H_{C2} , the $1/^{51}\text{T}_1$ stays nearly constant, for over one decade in temperature below 0.5 K, which clearly evidences gapless excitations. The 1DTFIM predicts $1/T_1 \sim T^{-0.75}$ at the QCP [14], while we observe a weakly T -dependent $1/T_1$ at H_{C2} . The deviation may arise if our measurement missed the exact H_{C2} , or if the temperature is not low enough. It is worth noting that for fields just below H_{C2} , the rapid drop of $1/T_1$ signals gapped excitations. This agrees with the prediction in the 1DTFIM, and to our knowledge, such a gap opening behavior has never been reported before.

We draw connections between our observations and the proposed topological phase transitions in $\text{BaCo}_2\text{V}_2\text{O}_8$ [27]. Although the materials are slightly different, the properties, especially the gapped excitations, in both the ordered phase at $H \ll H_C$ and the paramagnetic phase at $H \gg H_C$, are the same. However, when the 1D QCP is outside the 3D ordered phase, as in the case of $\text{SrCo}_2\text{V}_2\text{O}_8$, gapless excitations emerge at the two QCPs, since static linear confining potential is absent above H_{C1} . Moreover, an exposed 1D QCP outside the 3D ordered phase at a relatively low field promises an ideal approach for experimental investigation of the genuine 1D quantum criticality. For future studies, by rotating the field from [100] to [110] direction, two QCPs may be further separated, which allows accessing the quantum criticality of the 1DTFIM in a broader field range.

In summary, our NMR study in $\text{SrCo}_2\text{V}_2\text{O}_8$ reveals two separated quantum critical points experimentally with a transverse field, for the first time in this material. Our results also demonstrate distinctive quantum critical behaviors at the two QCPs, including the scaling behaviors of the transition/crossover temperatures and the spin dynamics. We propose that separate 1D and 3D QCPs are realized at very low fields, attributed to novel effects of the effective staggered magnetic field. Such a one-dimensional quantum critical point exposed outside the three-dimensional magnetic ordered phase at a low magnetic field opens a new avenue to access the genuine

quantum criticality of the one-dimensional transverse-field Ising model experimentally.

The authors acknowledge discussions with Prof. Bruce Normand. This work is supported by the Ministry of Science and Technology of China (Grant Nos. 2016YFA0300504 and 2016YFA0300503), the National Natural Science Foundation of China (Grant Nos. 51872328, 21875249, and 11674392, and 11804221), the Fundamental Research Funds for the Central Universities, the Research Funds of Renmin University of China (Grant Nos. 14XNLF08 and 18XNLG24), the Science and Technology Commission of Shanghai Municipality Grant No. 16DZ226020, and the Outstanding Innovative Talents Cultivation Funded Programs 2018 of Renmin University of China. JW acknowledges support from Shanghai city.

* Electronic address: hezz@fjirsm.ac.cn

† Electronic address: wujd@sju.edu.cn

‡ Electronic address: wgyu@phy@ruc.edu.cn

- [1] H. V. Loehneysen, *J. Low Temp. Phys.* **161**, 1 (2010).
- [2] S. Sachdev, *Quantum Phase Transitions* (Cambridge University Press, Cambridge, 2011).
- [3] P. Coleman and A. J. Schofield, *Nature (London)* **433**, 226 (2005).
- [4] P. Pfeuty, *Ann. Phys.* **57**, 79 (1970).
- [5] E. Barouch and B. M. McCoy, *Phys. Rev. A* **3**, 786 (1971).
- [6] R. Jullien, P. Pfeuty, J. N. Fields, and S. Doniach, *Phys. Rev. B* **18**, 3568 (1978).
- [7] J. H. H. Perk, H. W. Capel, G. R. W. Quispel, and F. W. Nijhoff, *Physica A* **123**, 1 (1984).
- [8] A. B. Zamolodchikov, *Int. J. Mod. Phys. A* **4**, 4235 (1989).
- [9] S. T. Carr and A. M. Tselik, *Phys. Rev. Lett.* **90**, 177206 (2003).
- [10] J. H. H. Perk and H. Au-Yang, *J. Stat. Phys.* **135**, 599 (2009).
- [11] J. Wu, M. Kormos, and Q. Si, *Phys. Rev. Lett.* **113**, 247201 (2014).
- [12] J. Wu, L. Zhu, and Q. Si, *Phys. Rev. B* **97**, 245127 (2018).
- [13] A. B. Zamolodchikov, *Int. J. Mod. Phys. A* **4**, 4235 (1989).
- [14] A. W. Kinross, M. Fu, T. J. Munsie, H. A. Dabkowska, G. M. Luke, S. Sachdev, and T. Imai, *Phys. Rev. X* **4**, 031008 (2014).
- [15] R. Coldea, D. Tennant, E. Wheeler, E. Wawrzynska, D. Prabhakaran, M. Telling, K. Habicht, P. Smeibidl, and K. Kiefer, *Science* **327**, 177 (2010).
- [16] S. Lee, R. K. Kaul, and L. Balents, *Nat. Phys.* **6**, 702 (2010).
- [17] Z. He, T. Taniyama, T. Kyomen, and M. Itoh, *Phys. Rev. B* **72**, 172403 (2005).
- [18] Z. He, T. Taniyama, and M. Itoh, *Phys. Rev. B* **73**, 212406 (2006).
- [19] S. Kimura, H. Yashiro, K. Okunishi, M. Hagiwara, Z. He, K. Kindo, T. Taniyama, and M. Itoh, *Phys. Rev. Lett.* **99**, 087602 (2007).
- [20] A. K. Bera, B. Lake, F. H. L. Essler, L. Vanderstraeten, C. Hubig, U. Schollwöck, A. T. M. N. Islam, A. Schneidewind, and D. L. Quintero-Castro, *Phys. Rev. B* **96**, 054423 (2017).
- [21] A. K. Bera, B. Lake, W.-D. Stein, and S. Zander, *Phys. Rev. B* **89**, 094402 (2014).
- [22] S. Kimura, T. Takeuchi, K. Okunishi, M. Hagiwara, Z. He, K. Kindo, T. Taniyama, and M. Itoh, *Phys. Rev. Lett.* **100**, 057202 (2008).
- [23] M. Klanjšek, M. Horvatić, S. Krämer, S. Mukhopadhyay, H. Mayaffre, C. Berthier, E. Canévet, B. Grenier, P. Lejay, and E. Orignac, *Phys. Rev. B* **92**, 060408(R) (2015).
- [24] S. Kimura, K. Okunishi, M. Hagiwara, K. Kindo, Z. He, T. Taniyama, M. Itoh, K. Koyama, and K. Watanabe, *J. Phys. Soc. Japan* **82**, 033706 (2013).
- [25] S. K. Niesen, G. Kolland, M. Seher, O. Breunig, M. Vallador, M. Braden, B. Grenier, and T. Lorenz, *Phys. Rev. B* **87**, 224413 (2013).
- [26] A. Okutani, S. Kimura, T. Takeuchi, and M. Hagiwara, *Appl. Magn. Reson.* **46**, 1003 (2015).
- [27] Q. Faure, S. Takayoshi, S. Petit, V. Simonet, S. Raymond, L. Regnault, M. Boehm, J. S. White, M. Månsson, C. Rüegg, P. Lejay, B. Canals, T. Lorenz, S. C. Furuya, T. Giamarchi, and B. Grenier, *Nat. Phys.* **14**, 716 (2018).
- [28] Z. Wang, J. Wu, S. Xu, W. Yang, C. Wu, A. K. Bera, A. T. M. Nazmul Islam, B. Lake, D. Kamenskyi, P. Gogoi, H. Engelkamp, N. Wang, J. Deisenhofer, and A. Loidl, *Phys. Rev. B* **94**, 125130 (2016).
- [29] Z. Wang, T. Lorenz, D. I. Gorbunov, P. T. Cong, Y. Kohama, S. Niesen, O. Breunig, J. Engelmayer, A. Herman, Jianda Wu, K. Kindo, J. Wosnitzer, S. Zherlitsyn, and A. Loidl, *Phys. Rev. Lett.* **120**, 207205 (2018).
- [30] M. Matsuda, H. Onishi, A. Okutani, J. Ma, H. Agrawal, T. Hong, D. M. Pajerowski, J. R. D. Copley, K. Okunishi, M. Mori, S. Kimura, and M. Hagiwara, *Phys. Rev. B* **96**, 024439 (2017).
- [31] S. Takayoshi, S. C. Furuya, and T. Giamarchi, *Phys. Rev. B* **98**, 184429 (2018).
- [32] The crystal information, *dc* magnetization data, the iTEBD results, the NMR lineshape discussions, and typical spin recovery curves are included in the supplemental materials.
- [33] D. E. MacLaughlin, J. D. Williamson, and J. Butterworth, *Phys. Rev. B* **4**, 60 (1971).
- [34] S. Wada, R. Aoki, and O. Fujita, *J. Phys. F: Met. Phys.* **14**, 1515 (1984).
- [35] S. K. Niesen, O. Breunig, S. Salm, M. Seher, M. Vallador, P. Warzanowski, and T. Lorenz, *Phys. Rev. B* **90**, 104419 (2014).
- [36] Y. Kawasaki, Y. Ideta, Y. Kishimoto, T. Ohno, K. Omura, T. Fujita, S. Kimura, and M. Hagiwara, *J. Phys. Soc. Japan* **3**, 014001 (2014).
- [37] Z. Wang, M. Schmidt, A. K. Bera, A. T. M. N. Islam, B. Lake, A. Loidl, and J. Deisenhofer, *Phys. Rev. B* **91**, 140404 (2015).
- [38] R. Orús and G. Vidal, *Phys. Rev. B* **78**, 155117 (2008).
- [39] A. Okutani, T. Kida, T. Usui, T. Kimura, K. Okunishi, and M. Hagiwara, *Phys. Procedia* **75**, 779 (2015).